ISSN 1990-7931, Russian Journal of Physical Chemistry B, 2016, Vol. 10, No. 1, pp. 100–108. © Pleiades Publishing, Ltd., 2016.
Original Russian Text © M.V. Klimenko, V.V. Klimenko, I.E. Zakharenkova, 2016, published in Khimicheskaya Fizika, 2016, Vol. 35, No. 1, pp. 31–40.

CHEMICAL PHYSICS OF ATMOSPHERIC PHENOMENA

Longitudinal Variations of the Ionospheric, Plasmaspheric, and Total Electron Contents in December 2009

M. V. Klimenko[a, b, *], V. V. Klimenko[a], and I. E. Zakharenkova[a]

[a] *Western Department of Pushkov Institute of Terrestrial Magnetism, Ionosphere, and Radio Waves Propagation, Russian Academy of Sciences, Kaliningrad, Russia*

[b] *Kant Baltic Federal University, Kaliningrad, Russia*

**e-mail: maksim.klimenko@mail.ru*

Received March 17, 2015

Abstract—The major morphological features of the global structure and longitudinal variations of the electron content distribution in the ionosphere–protonosphere system during the winter solstice for the solar activity minimum in 2009 are examined. It is demonstrated how the Weddell Sea anomaly and the longitudinal structure of the main ionospheric trough (depression in the concentration of light ions) manifest themselves through the total, ionospheric, and protonospheric electron contents. Based on model calculations, the specific features of longitudinal variations in the O^+/H^+ transition altitude are for the first time considered, which made it possible to estimate the altitude of the transition boundary from the ionosphere to the plasmasphere (protonosphere) for the selected conditions.

Keywords: ionosphere, plasmasphere, protonosphere, longitudinal variations, electron content, main ionospheric trough, Weddell Sea anomaly

DOI: 10.1134/S1990793116010085

1. INTRODUCTION

It is known that, due to the offset between the geographic and geomagnetic axes [1], as well as the existence of longitudinal variations of the parameters of the lower and middle atmosphere [2], the ionospheric parameters at all latitudes exhibit a significant longitudinal variability, comparable to the diurnal variations of these parameters. Studies of longitudinal variations of the electron density in the ionosphere were conducted mainly based on satellite-collected data, since it is satellite measurements that make it possible to describe variations of the ionospheric parameters in all corners of our planet. For this purpose, data from different satellites, such as, e.g., Ariel [3], IC-19 [4–6], TOPEX [7–9], DMSP [10], and CHAMP [11], have been used. Recently, longitudinal variations of the ionosphere parameters have been studied based on radio occultation data from the COSMIC low-orbit satellite constellation [12–14], as well as data obtained by the tomography method implemented using low-orbit satellites and navigation satellite positioning systems [15]. The authors of [16] reported the results of investigation of the latitudinal structure of the longitudinal variations of the thermospheric, ionospheric, and electrodynamic parameters at different altitudes based on satellite data. This made it possible to clearly demonstrate the relationship between the longitudinal variations of the parameters of the thermosphere and electric field with the longitudinal variability of the F2 region of the ionosphere and the total electron content. All these studies show that the longitudinal variation manifests itself most clearly during solstice periods in both the summer and winter hemispheres. This is evidenced by the presence of a significant longitudinal variation of the main ionospheric trough in the winter hemisphere, crests of the equatorial anomaly, as well as the formation of the Weddell Sea anomaly in the southern hemisphere and the Yakutsk anomaly in the northern hemisphere in the summertime, which manifest themselves in the form of abnormal diurnal variations, with the nighttime values exceeding the daytime only in the Yakutsk and American longitudinal sectors.

Researchers of the ionosphere, based on the assumption of a small contribution of the plasmasphere to the total electron content, normally identify variations of the total electron content (TEC) from the Earth's surface to the an altitude of ~20200 km, as measured by the GLONASS/GPS systems, with variations of the electron density N_mF2 in the maximum of the F2 layer, as obtained by sounding the ionosphere. However, quite often, this view turns out to be wrong. Research in this direction has been actively carried out immediately after the commissioning of the GPS satellite navigation system. In most previous studies, the contribution from the plasmasphere to the TEC has been evaluated only in a limited range of longitudes and latitudes [17–22]. There are only a small number

of studies that have attempted to find the answer to this question on a global scale [23–25]. Note that the knowledge about the longitudinal variability of the plasmasphere is still limited. Only a few works have been devoted to longitudinal variations of plasmaspheric parameters [26, 27], in a limited region of space at that. Only the authors of [25] touched the unsolved problem of longitudinal variations of the plasmaspheric parameters at all latitudes. The solution of this problem is important for refining the positioning method in the case of using single-frequency receivers of signals from GLONASS/GPS navigation satellites at different latitudes and longitudes.

The aim of the present work is to identify and study the basic morphological features of the global structure and longitudinal variations of the electron content distribution in the ionosphere–plasmasphere system during the winter solstice for the minimum of the solar activity in 2009. This article is intended to continue the series of our work on this subject [28, 29], carried out using the Global Self-Consistent Model of the Thermosphere, Ionosphere, and Protonosphere (GSM TIP) and satellite measurements of the ionospheric and plasmaspheric parameters. Achieving this goal will help form a view about the manifestations of the Weddell Sea anomaly and the longitudinal variation of the main ionospheric trough in the integrated content of the ionosphere and plasmasphere individually and in the entire system as a whole. Also, based on model calculations, this article for the first time examines the specific features of longitudinal variations in the altitude of the O^+/H^+ transition, which makes it possible to estimate the altitude of the boundary of the transition from the ionosphere to the plasmasphere under these particular conditions.

2. DESCRIPTION OF THE GSM TIP

The parameters of the ionosphere–plasmasphere system were numerically calculated using the GSM TIP [30, 31], developed at Western Department of Pushkov Institute of Terrestrial Magnetism, Ionosphere, and Radio Waves Propagation of the Russian Academy of Sciences, and modified in the part concerning the calculation of the electric fields of dynamo and magnetospheric origin [32–34]. The GSM TIP calculates time-dependent three-dimensional global distributions of the temperature, composition (O_2, N_2, O), and neutral gas velocity vector, as well as the concentration, temperature, velocity vectors of atomic (O^+, H^+) and molecular (N_2^+, O_2^+, NO^+) ions and electrons, along with two-dimensional distributions of the electric potential of both ionospheric and magnetospheric origins. All the equations of the model are solved by the finite difference method.

In the GSM TIP, the geomagnetic field of the Earth is approximated by a central dipole. The model takes into account the setoff between the geographical and geomagnetic axes, which makes it possible to describe the evolution of the longitudinal structure of the parameters of the thermosphere–ionosphere system. Note, however, that the use of the dipole approximation in the GSM TIP instead of the actual geomagnetic field prohibits reproducing the real longitudinal variations of the ionospheric parameters, especially in the northern hemisphere, where the differences between the real geomagnetic field and its dipole approximation are greatest. By contrast, in the southern hemisphere, the dipole approximation is much less different from the actual distribution of the geomagnetic field, which makes it possible to describe in detail the longitudinal variability of the ionosphere in the southern hemisphere and, in particular, one of the most interesting features of the summer southern hemisphere, the Weddell Sea anomaly. Unfortunately, at the current stage of development of the GSM TIP, it cannot reproduce the actual geomagnetic field, because it would require constructing a completely new model. We believe that, to understand the essence of the processes involved in the formation of the longitudinal distribution of the parameters of the ionosphere–plasmasphere system, it suffices to use the dipole approximation of the geomagnetic field, which is implemented in the current version of the GSM TIP.

Note that, in most existing models of the ionosphere, various characteristics of the near-Earth environment, such as the conductivity, electric field strength, composition, thermal mode, and dynamics the neutral atmosphere are input parameters; i.e., are set based on empirical models. In contrast to such models, all the GSM TIP parameters are calculated self-consistently. The modification of the GSM TIP performed in recent years makes it possible to correctly describe the distribution of the electric field, zonal current, and other ionospheric parameters at low latitudes and at the geomagnetic equator, as well as to use modern models of high-energy electron precipitation. To carry out this study in quiet geomagnetic conditions, we performed calculations for the conditions of the winter solstice (December 22, 2009) at a low solar and geomagnetic activity, without regard for thermospheric tides at the low boundary of the GSM TIP. Note that the chosen day is best suited for studying the ionosphere–plasmasphere system in quiet conditions, since the geomagnetic activity throughout 2009 was very low, so that we are to deal with a filled plasmasphere.

3. SATELLITE OBSERVATIONS OF THE ELECTRON CONTENT IN THE IONOSPHERE–PLASMASPHERE SYSTEM

Experimental basis of this study is a set of radio occultation measurement data collected by FORMOSAT-3/COSMIC low-orbit satellites (hereinafter, COSMIC), as well as data from the global network of ground-

based receivers of signals from the GLONASS/GPS navigation system. Thus, in this project, we implemented an integrated approach to studying the ionosphere–plasmasphere system using global-scale model calculations and multi-instrumental experimental data.

3.1. Determination of the TEC from Data Collected by a Network of Ground-Based Receivers of Signals from the Satellite Navigation Systems

To date, the method for measuring the delay signals from global navigation satellite systems (GNSS), such as GPS and GLONASS, is one of the main methods of obtaining information on the global state of the ionosphere–plasmasphere system. The TEC of the ionosphere obtained in this way is a very convenient parameter for analyzing the variability of the ionosphere on the global and regional scales. A dense network of ground-based GNSS receivers makes it possible to carry out continuous and regular monitoring of the global (regional) TEC distributions with a high temporal resolution. On-ground GNSS measurements provide information on the total electron content in the column from the base of the ionosphere to the orbit altitude of the navigation satellites (20200 km), which, however, does not make it possible to determine the total electron content in the ionosphere and the plasmasphere separately. The sources of errors in constructing TEC maps are the assumption of spherical symmetry in the conversion of the measured inclined TEC to the vertical TEC, especially at low angles of elevation, evaluation the differential code bias (DCB), interpolation in constructing the map; slip cycle, multibeam mode, pseudonoise range, etc.

Global TEC maps are regularly published by four independent centers of the international geodynamic service (IGS), using different technologies and data from different sets of stations [35]. In the present study, we used the final product of the IGS, which is a resulting global TEC map constructed from a combination of four other products. Global TEC maps are drawn with a spatial resolution of 5° in longitude and 2.5° in latitude at a time step of 1–2 h. We used standard TECU units (1 TECU = 10^{12} cm^{-2}). It should be noted that the vertical TEC data derived from GIMs maps are currently determined with a sufficiently good accuracy over areas with a regularly operating GNSS network, being, of course, less accurate over oceans, deserts, and in high latitudes.

3.2. Radio Occultation GPS COSMIC Monitoring of the Ionosphere

In this study, we used radio occultation data from the COSMIC low-orbiting satellites and published by the CDAAC (COSMIC data analysis and archive center, http://www.cosmic.ucar.edu/cdaac/). The result of a session of radio occultation measurements between the GPS receiver on a COSMIC satellite (at an orbital altitude of ~800 km) and a GPS transmitter (at an orbital altitude of 20200 km) is a set of TEC measurements along beams successively intersecting the ionosphere from ~800 to 80–100 km. At the CDAAC, ionospheric electron density profiles are derived from a series of TEC measurements by using the Abel inversion under a number of assumptions, including that of the ionosphere being spherically symmetric, which is the most significant source of errors. The Abel inversion can lead to significant errors for low latitudes and low altitudes. A detailed description of how CDAAC data are obtained and of the method of recovery of the electron density profile N_e can be found in [36].

We used the second level of the data provided by the CDAAC, namely "ionprf" files, which contain information on vertical electron density profiles. We carried out an additional analysis of data quality to identify and remove bad or questionable data, more specifically, vertical electron density profiles with large heterogeneous overshoots and gaps. For this purpose, we carefully examined the shapes of the profile and the rate of change of the electron density under preset constraints.

To estimate the ionospheric electron content (IEC), we integrated the COSMIC-published vertical profiles of the electron density in the ionosphere. The upper integration limit was set at 800 km (orbit altitude of COSMIC satellites). Thus, the IEC is the electron concentration integrated over the altitudes of 100 to 800 km. Note that, in some areas at some local times, the relative error in determination of the IEC can reach ~50%. All the IEC values for December 2009 were collected and divided into 12 time 2-h intervals. To estimate the global IEC distribution, we expansion in spherical harmonics from the 1st to the 15th terms. The resulting map was a distribution of month-averaged IEC values. This, for December 2009, we produced 12 maps of averaged IEC values drawn at 2-h time intervals with a spatial resolution similar to GPS TEC maps (2.5° in latitude and 5° in longitude). One advantage of COSMIC data is a good coverage of the Earth's surface with radio occultation measurements, including areas without land-based means of measurements. The average number of electron density profiles obtained per day from COSMIC data is 1500–2500. To construct the maps for December 2009, we selected and processed over 58000 vertical electron density profiles. It should be noted that the joint use of data from low-orbit satellites and from navigation system satellites for studying longitudinal variations of ionospheric and total electron content makes it possible to estimate the longitudinal variations of the plasmaspheric electronic content.

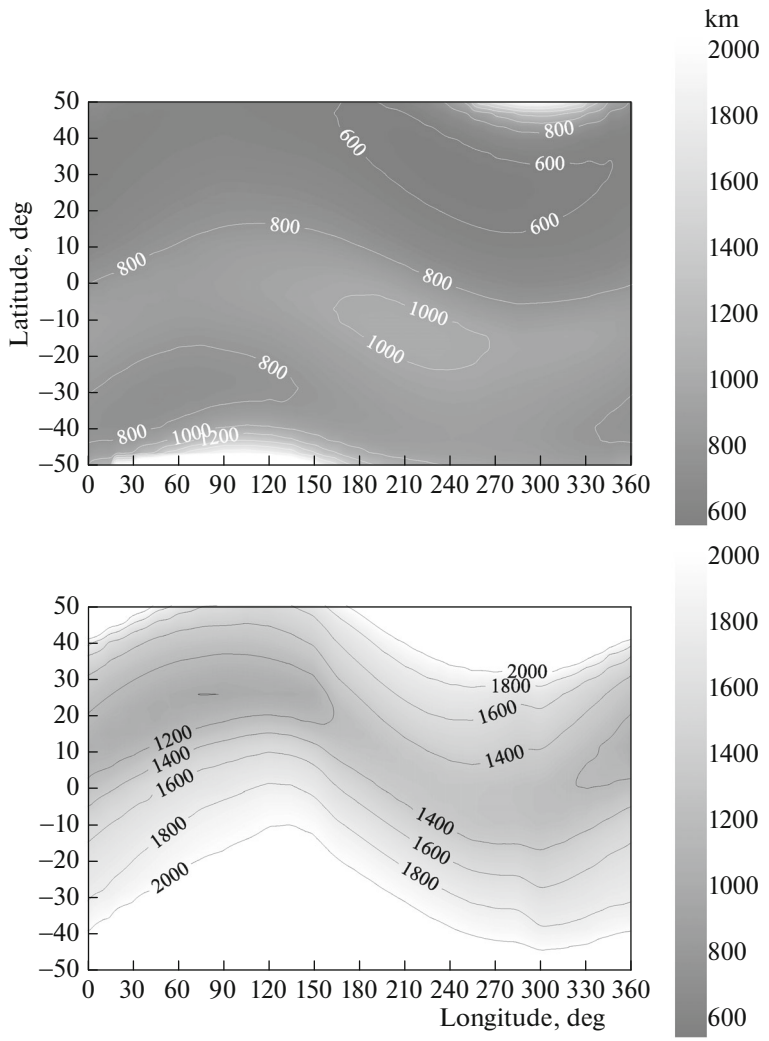

Fig. 1. Maps of longitudinal variations of the O^+/H^+ transition altitude in the range of latitudes from 50° S to 50° N as calculated using the GSM TIP for 24:00 (top) LT and 12:00 LT (bottom) December 22, 2009.

4. RESULTS

To begin with, let us define the conditional boundary between the ionosphere and the plasmasphere. The altitude of the O^+/H^+ transition is a natural boundary between the ionosphere and the plasmasphere (protonosphere). Below the transition altitude is located the ionosphere, with the main peak of the F2 layer being formed by O^+ ions. At the same time, the O^+/H^+ transition altitude is the lower boundary of the plasmasphere (protonosphere), which is dominated by H^+ ions. To date, there is a number of works that examined this parameter under conditions of a long abnormal minimum of solar activity in 2007–2009 [29, 37–39]. These studies showed that, at the O^+/H^+ transition altitude near the equator can reach ~450 km, which is very close to the altitude of the maximum of the F region of the ionosphere. Figure 1 shows a map of longitudinal variations of the O^+/H^+ transition altitude calculated by the GSM TIP for 24:00 LT and 12:00 LT December 22, 2009. This figure shows that, at midnight, the altitude of the transition is much lower than in the afternoon. At nighttime, the minimum altitude of the transition, 570 km, is reached in the northern hemisphere at a latitude of 30° N and a longitude of 240° E, while at the same local time, the maximum transition altitude is 2000 km or more, near latitudes of ±50° at a longitude of 105° E in the southern hemisphere and a longitude of 300° E in the northern hemisphere. At noon, the minimum altitude of the transition increases to 1000 km in the northern hemisphere, at the latitude of 25° N and longitude 75° E. In the daytime, the maximum transition altitude of 2000 km and more sets in over a large area in the northern and, especially, in the southern hemisphere. That the transition altitude at the daytime is greater than at the nighttime can be explained by the fact that, at the daytime, the concentration of O^+ ions in the maximum of the F2 layer and above is higher due to the emergence of ionization sources associated

with solar radiation, a factor not operative in the case of H^+ ions, which are formed in the charge-exchange reaction between O^+ ions and hydrogen atoms. Note that the low calculated values of the transition altitude for the nighttime conditions are associated with very low levels of solar activity over the indicated period, as evidenced by the results of observations and simulations [37–39]. As for the longitudinal variation of the O^+/H^+ transition altitude, arising because of the offset between the geographic and geomagnetic poles, it clearly manifests one maximum and one minimum at all latitudes in the night- and daytime. Transition altitude maps for the nighttime conditions clearly show a difference between the longitudinal variations in the winter (northern) summer and (southern) hemisphere. For example, the longitudinal variation in the winter hemisphere exhibits significant changes in the transition altitude at fixed latitudes, whereas in the summer hemisphere, on the contrary, these changes are small. For the daytime conditions, the longitudinal variations in the different hemispheres do not differ from each other.

Figure 2 shows the global (TEC), ionospheric (IEC) and plasmaspheric (PEC) electron contents calculated within the framework of the GSM TIP for 6:00, 12:00, 18:00 and 24:00 UT December 22, 2009. The total electron content is calculated in the model by integrating the electron density over a vertical column from 80 km (lower boundary altitude for the GSM TIP) to 20000 km (orbital altitude of GPS and GLONASS satellites). To be correct, the ionospheric electron content should be calculated to the O^+/H^+ transition altitude; however, to compare the results with observational data, we fixed the upper limit of integration at 800 km, as was done in [40]. Thus, in the mid-latitudes, we underestimate the IEC, especially for the daytime, when the transition altitude is much greater than 800 km. The plasmaspheric electron content was calculated as the difference between the total and the ionospheric electron content. These maps show UT variations of the main ionospheric trough in the northern (winter) hemisphere in IEC and the light ion trough in PEC, as well as manifestations thereof in the TEC. A set of global TEC, IEC, and PEC maps for different moments of UT makes it possible to trace the dynamics of changes in the electron density in the ionosphere–protonosphere system associated with manifestations of longitudinal variation in this system. For example, the global TEC, IEC, and PEC maps for December 2009 presented in [24], drawn based on GPS-TEC and COSMIC observations, show an abnormally high electron concentration in the Weddell Sea area at 6:00 UT and 00:00 UT, when the main source of ionization, ultraviolet radiation from the sun, is absent, which however, is not discussed in this article. Note that the behavior of the ionosphere above the Weddell Sea attracted the attention of scientists many years ago, as the Halley Bay and Argentine Island mid-latitude ionospheric stations, located in the Southern Hemisphere, detected an abnormal behavior of *fo*F2 during the period from December to February 2009, when the nighttime values of *fo*F2 exceeded those at the daytime [41, 42]. This effect was called the Weddell Sea anomaly (WSA). The IEC maps drawn based on GSM TIP calculations (Fig. 2) clearly show the formation of high nighttime IEC values near the Weddell Sea in the southern (summer) hemisphere at latitudes of 60°–75° S near a longitude of 285° E (75° W). The same UT variation manifests itself on TEC and PEC maps. One can see a close agreement of the model calculations with the observational data reported in [24]. For better perception of longitudinal TEC, IEC and PEC variations, it is worthwhile to change to a different presentation of the simulation results.

Figure 3 shows global maps of the longitudinal TEC, IEC, and PEC variations calculated in the framework of the GSM TIP for 12:00 LT and 24:00 LT December 22, 2009. A comparison of the daytime TEC map with the nighttime one shows that, near the longitude of 285° E (75° W) in the southern (summer) hemisphere at latitudes from ~70° S to the South Pole, the nighttime TEC values exceed those observed in the daytime, with the maximum excess of the daytime value over the nighttime value being ~1.5 TECU. It is a manifestation of the Weddell Sea anomaly through the TEC value. Note that, in the daytime at the same latitudes in the longitudinal range of 40° E–150° E, the longitudinal TEC distribution also features a maximum, however, with a magnitude smaller than that characteristic of the nighttime TEC in the WSA. Note that, during the daytime in the same area, a minimum appears in the longitudinal TEC distribution. Another interesting feature of the presented TEC distributions is a longitudinal variation of the main ionospheric trough in the northern (winter) hemisphere, which change from day to night. In the daytime, the longitudinal variation of the TEC depression has a distinct single-wave structure with a maximum at a longitude of 170° E and a minimum at 90° E, related to the geographic coordinate system. The manifestation of the main ionospheric TEC trough in the nighttime also has a single-wave structure, but related to the geomagnetic field, which is evident from its formation along the geomagnetic parallels.

Finally, the third feature of the longitudinal TEC variation is a longitudinal variation of the equatorial anomaly, which is of dual nature. Firstly, it has a distinct single-wave structure related to the geographic coordinate system, with a maximum at longitude 320° E and a minimum at 150° E in the daytime, which change, respectively, to 180° E and 300° E in the nighttime. Secondly, it has a distinct single-wave structure related to the geomagnetic coordinate system and formed along the geomagnetic latitude in the day- and nighttime. Note also the absence of the winter anomaly in the longitudinal TEC variations.

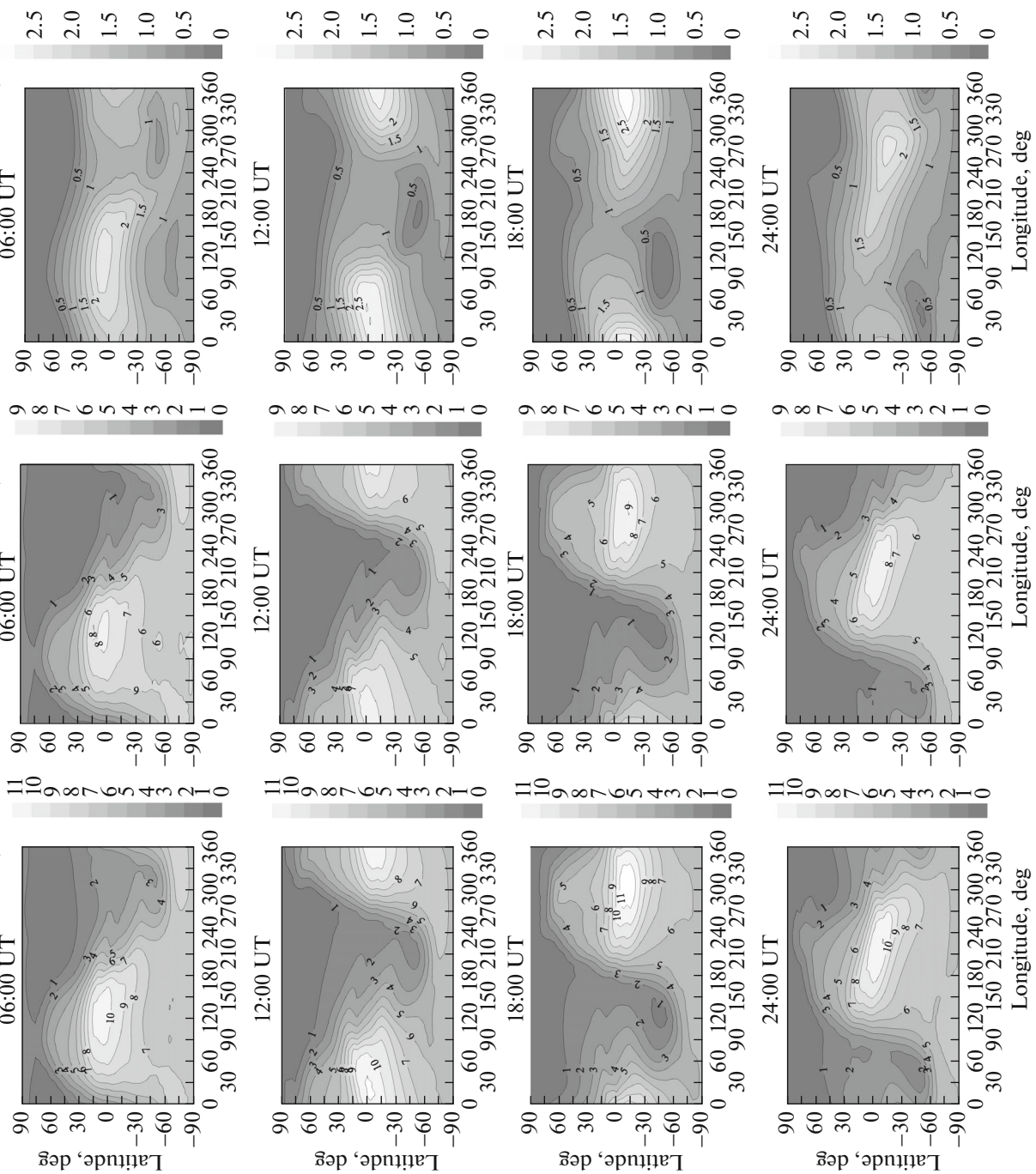

Fig. 2. Global maps of the TEC, IEC, and PEC (left to right) calculated within the framework of the GSM TIP for 06:00 UT, 12:00 UT, 18:00 UT and 24:00 UT (top to bottom) December 22, 2009.

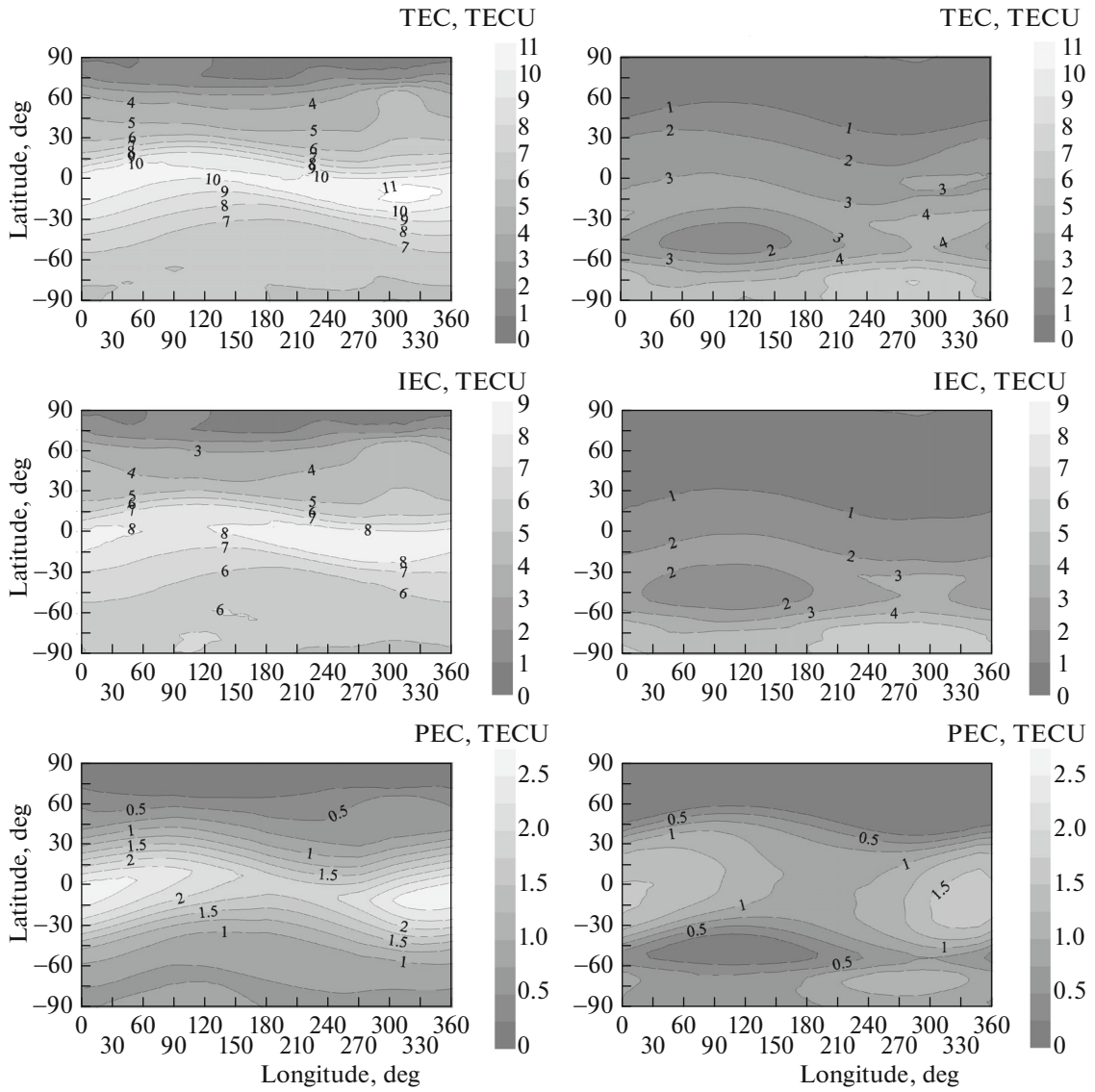

Fig. 3. Global maps of longitudinal variations of the TEC, IEC, and PEC, calculated by the GSM TIP for 12:00 LT (left) and 24:00 LT (right) December 22, 2009.

The longitudinal IEC variation is very similar to the longitudinal TEC variations, differing from it only by a longitudinal displacement the maximum and minimum in the equatorial anomaly region. A distinctive feature of the longitudinal PEC variation is the disappearance of its dependence on the geographic coordinate system in the equatorial anomaly region and the presence of a distinct single-wave structure dependent on the geomagnetic field. Furthermore, it should be noted that the WSA manifests itself through the PEC more clearly than through the TEC and IEC.

To compare the simulation results with the observed behavior of the TEC, IEC, and PEC, we used the data described in Section 3 of this article. Figure 4 shows global maps of longitudinal TEC variations drawn based on data from a network of ground-bases receivers of GPS satellite signals. The IEC maps were constructed using radio occultation measurement data from COSMIC satellites, whereas the PEC maps were drawn as the difference between the results of measurements of the TEC and IEC at 12:00 LT and 24:00 LT December 22, 2009. It should be noted that the longitudinal variations calculated by the GSM TIP are severalfold lower than the observed. For example, according to GPS measurements, the difference between the nighttime and daytime values of the TEC in the WSA is ~ 4 TECU. In the equatorial anomaly region, the maximum and minimum are located, respectively, at longitudes of 0° E and 300° E in the daytime and at 0° E and 210° E in the nighttime. In addition, the measurement data not so clearly demonstrate the relation of the equatorial anomaly with the geomagnetic field, which apparently is due to the existence of a stronger relation of the longitudinal TEC vari-

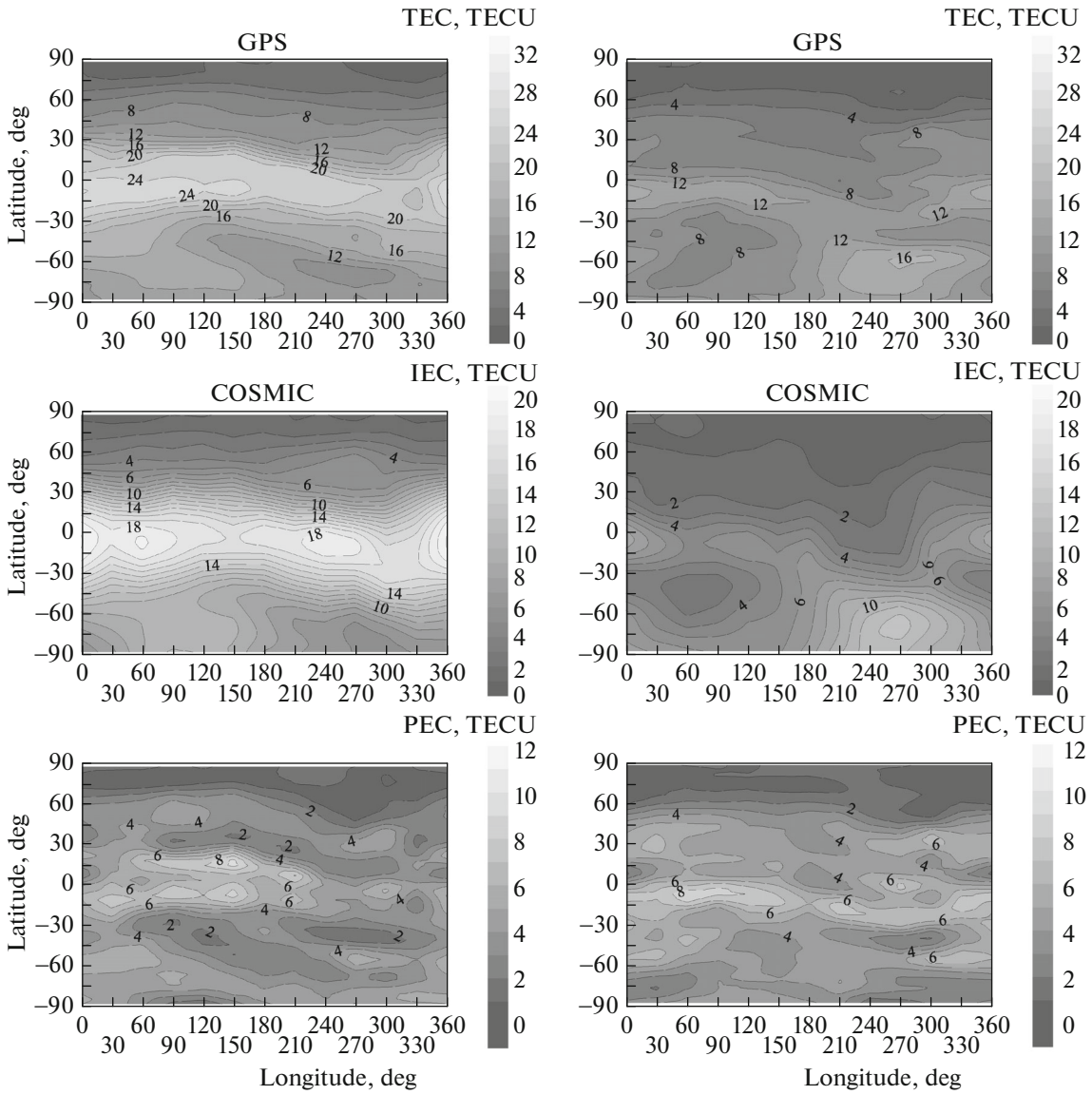

Fig. 4. Global maps of longitudinal variations of the TEC, IEC, and PEC drawn based on observational data from a network of ground-based receivers of signals from GPS and COSMIC satellites for 12:00 LT (left) and 24:00 LT (right) December 22, 2009.

ation in this area with the geographic coordinate system. The same applies to the longitudinal TEC variations in the region of the main ionospheric trough.

In contrast to the simulation results, the longitudinal IEC variation in the region of the equatorial anomaly has a distinct two-wave structure In our opinion, this difference between observational data and modeling results arises due to the use of the dipole approximation for the geomagnetic field. According to the COSMIC measurement, the difference between nighttime and daytime values of the IEC in the WSA region is ~6 TECU, which exceeds the value of this quantity obtained from GPS measurements.

In contrast to the simulation results, the experimentally determined longitudinal PEC variation reveals a well-pronounced small-scale structure associated, in our view, with the different accuracy of measurements of the TEC and IEC values, despite a sufficient smoothness of the initial data. In addition, the measured PEC also features the Weddell Sea anomaly, in which the difference between the nighttime and daytime values of PEC is ~1 TECU.

5. CONCLUSIONS

Thus, based on modeling simulations and satellite observations, we identified the main morphological features of the global structure and longitudinal variations of the electronic content distribution in the ionosphere–plasmasphere system in the period of the winter solstice at the solar activity minimum in 2009. The longitudinal variation of the O^+/H^+ transition

altitude clearly manifests itself at all latitudes in the night- and daytime, being associated with the longitudinal variation arising because of the offset between the geographic and geomagnetic poles. Also is shown how the Weddell Sea anomaly and the longitudinal structure of the main ionospheric trough (depression in the concentration of light ions) manifest themselves through the total, protonospheric, and ionospheric electron contents. According to the model calculations, the longitudinal variation in the plasmaspheric electron content reflects the relationship between the longitudinal variation in the ionosphere–plasmasphere system and the offset between the geographic and geomagnetic axes.

ACKNOWLEDGMENTS

We grateful to the IGS for providing GPS data and products (ftp://cddis.gsfc.nasa.gov/pub/gps/products/ionex) and the CDAAC for COSMIC data (http://www.cosmic.ucar.edu/cdaac/).

The work was supported by grants of the President of the Russian Federation (MK-4866.2014.5; M.V. Klimenko, I.E. Zakharenkova) and the Russian Foundation for Basic Research, project no. 14-05-00788 (V.V. Klimenko). The work was conducted under the project "Physical Mechanisms of the Formation of the Response of the Upper Atmosphere and Ionosphere to the Processes in the Lower Atmosphere and on the Earth's Surface" (Ministry of Education and Science of the Russian Federation, state contract no. 3.1127.2014/K).

REFERENCES

1. M. A. Knyazeva, Yu. V. Zubova, and A. A. Namgaladze, Vest. MGTU **13**, 1068 (2010).
2. M. E. Hagan and J. M. Forbes, J. Geophys. Res. D **107** (24), 21 (2002).
3. D. Eccles, J. W. King, and P. Rothwell, J. Atmosph. Terr. Phys. **33**, 371 (1971).
4. N. A. Kochenova, Geomagn. Aeron. **27**, 142 (1987).
5. M. G. Deminov and A. T. Karpachev, Geomagn. Aeron. **27**, 76 (1987).
6. A. T. Karpachev, Geomagn. Aeron. **28**, 46 (1988).
7. I. Horvath, J. Geophys. Res. A **111**, 12317 (2006). doi: 10.1029/2006JA011679
8. L. Scherliess, D. C. Thompson, and R. W. Schunk, J. Geophys. Res. A **113**, 01311 (2008).
9. G. Jee, A. G. Burns, Y.-H. Kim, et al., J. Geophys. Res. A **114**, 04307 (2009). doi: 10.1029/2008JA013801
10. I. Horvath and B. C. Lovell, J. Geophys. Res. A **114**, 02306 (2009). doi: 10.1029/2008JA013719
11. H. Liu, S. V. Thampi, and M. Yamamoto, J. Geophys. Res. A **115**, 01305 (2010). doi: 10.1029/2009JA014689
12. C. H. Lin, C. C. Hsiao, J. Y. Liu, and C. H. Liu, J. Geophys. Res. A **112**, 12305 (2007).
13. M. He, L. Liu, W. Wan, et al., J. Geophys. Res. A **114**, A12309 (2009). doi: 10.1029/2009JA014175
14. G. Liu, T. J. Immel, S. L. England, K. K. Kumar, and G. Ramkumar, J. Geophys. Res. A **115**, A04303 (2010).
15. S. Thampi, C. H. Lin, H. Liu, et al., J. Geophys. Res. A **114**, A10318 (2009). doi: 10.1029/2009JA014439
16. E. Yizengaw, Int. J. Geophys. **2012**, 342581 (2012). doi: 10.1155/2012/342581
17. N. Lunt, L. Kersley, and G. J. Bailey, Radio Sci. **34**, 725 (1999). doi: 10.1029/1999RS900002
18. N. Balan, Y. Otsuka, T. Tsugawa, et al., Earth Planets Space **54**, 71 (2002).
19. A. Belehaki, N. Jakowski, and B. W. Reinisch, Adv. Space Res. **33** (6) (2004). doi: 10.1029/1999RS900002
20. M. Moser, M. Gende, C. Brunini, R. Ezquer, and D. Altadill, Adv. Space Res. **39**, 841 (2007).
21. G. Manju, S. Ravindran, C. V. Devasia, S. V. Thampi, and R. Sridharan, J. Atmosph. Sol.-Terr. Phys. **70**, 1066 (2008).
22. I. E. Zakharenkova, Iu. V. Cherniak, A. Krankowski, and I. I. Shagimuratov, Adv. Space Res. **52**, 1827 (2013). doi: 10.1016/j.asr.2012.09.043
23. E. Yizengaw, M. B. Moldwin, D. Galvan, et al., J. Atmosph. Sol.-Terr. Phys. **70**, 1541 (2008).
24. Yu. V. Cherniak, I. E. Zakharenkova, A. Krankowski, and I. I. Shagimuratov, Adv. Space Res. **50**, 427 (2012).
25. H. B. Lee, G. Jee, Y. H. Kim, and J. S. Shim, J. Geophys. Res. **118**, 935 (2013). doi: 10.1002/jgra.50130
26. M. A. Clilverd, N. P. Meredith, R. B. Yorne, et al., J. Geophys. Res. A **112**, 11210 (2007). doi: 10.1029/2007JA012416
27. F. W. Menk, S. T. Ables, R. S. Grew, M. A. Clilverd, and B. R. Sandel, J. Geophys. Res. A **117**, 03215 (2012). doi: 10.1029/2011JA017071
28. V. V. Klimenko, A. T. Kapachev, and M. V. Klimenko, Russ. J. Phys. Chem. B **7**, 611 (2013). doi: 10.7868/S0207401X13090070
29. M. V. Klimenko, V. V. Klimenko, I. E. Zakharenkova, and Yu. V. Cherniak, Adv. Space Res. **55**, 2077 (2015). doi: 10.1016/j.asr.2014.06.027
30. A. A. Namgaladze, Yu. N. Korenkov, V. V. Klimenko, et al., Pure Appl. Geophys. (PAGEOPH) **127**, 219 (1988).
31. A. A. Namgaladze, Yu. N. Koren'kov, V. V. Klimenko, et al., Geomagn. Aeron. **30**, 612 (1990).
32. V. V. Klimenko, M. V. Klimenko, and V. V. Bryukhanov, Mat. Model. **18** (3), 77 (2006).
33. M. V. Klimenko, V. V. Klimenko, and V. V. Bryukhanov, Geomagn. Aeron. **46**, 457 (2006).
34. M. V. Klimenko, V. V. Klimenko, and V. V. Bryukhanov, Adv. Radio Sci. **5**, 385 (2007).
35. M. Hernández-Pajares, J. M. Juan, J. Sanz, et al., J. Geodesy. **83**, 263 (2009). doi: 10.1007/s00190-008-0266-1
36. Y.-H. Kuo, T. Wee, S. Sokolovskiy, et al., J. Meteorolog. Soc. Jpn. **82** (1B), 507 (2004).
37. R. A. Heelis, W. R. Coley, A. G. Burrell, et al., Geophys. Rev. Lett. **36**, L00C03 (2009). doi: 10.1029/2009GL038652
38. N. Balan, C. Y. Chen, J. Y. Liu, and G. J. Bailey, Ind. J. Radio Space Phys. **41**, 89 (2012).
39. N. Balan, C. Y. Chen, P. K. Rajesh, J. Y. Liu, and G. J. Bailey, J. Geophys. Res. A **117**, 08316 (2012). doi: 10.1029/2012JA017846
40. N. M. Pedatella, J. M. Forbes, A. Maute, et al., J. Geophys. Res. A **116**, 12309 (2011). doi: 10.1029/2011JA016600
41. W. H. Bellchambers and W. R. Piggott, Nature **182**, 1596 (1958).
42. R. Penndorf, Antarct. Res. Ser. **4**, 1 (1965).

Translated by V. Smirnov